

**1 The impact of the Kasatochi eruption on the Moon's**  
**2 illumination during the August 2008 lunar eclipse**

A. García Muñoz,<sup>1,2</sup> E. Pallé,<sup>1,2</sup> M.R. Zapatero Osorio,<sup>3</sup> and E.L. Martín<sup>3</sup>

arXiv:1106.3050v1 [astro-ph.EP] 15 Jun 2011

---

<sup>1</sup>Instituto de Astrofísica de Canarias  
(IAC), C/ Vía Láctea s/n, E-38200 La  
Laguna, Tenerife, Spain

<sup>2</sup>Departamento de Astrofísica,  
Universidad de La Laguna (ULL), E-38206  
La Laguna, Tenerife, Spain

<sup>3</sup>Centro de Astrobiología, CSIC-INTA,  
Madrid, Spain

3 The Moon's changeable aspect during a lunar eclipse is largely attributable  
4 to variations in the refracted unscattered sunlight absorbed by the terres-  
5 trial atmosphere that occur as the satellite crosses the Earth's shadow. The  
6 contribution to the Moon's aspect from sunlight scattered at the Earth's ter-  
7 minator is generally deemed minor. However, our analysis of a published spec-  
8 trum of the 16 August 2008 lunar eclipse shows that diffuse sunlight is a ma-  
9 jor component of the measured spectrum at wavelengths shorter than 600  
10 nm. The conclusion is supported by two distinct features, namely the spec-  
11 trum's tail at short wavelengths and the unequal absorption by an oxygen  
12 collisional complex at two nearby bands. Our findings are consistent with  
13 the presence of the volcanic cloud reported at high northern latitudes fol-  
14 lowing the 7–8 August 2008 eruption in Alaska of the Kasatochi volcano. The  
15 cloud both attenuates the unscattered sunlight and enhances moderately the  
16 scattered component, thus modifying the contrast between the two contri-  
17 butions.

## 1. Introduction

18 The classical theory of lunar eclipses accounts for refraction, differential absorption and  
19 focusing to explain the Moon's aspect during an eclipse [*Link*, 1962]. Link's classical the-  
20 ory has been subsequently perfected and used to investigate the composition and aerosol  
21 loading of the Earth's atmosphere [e.g., *Ugolnikov and Maslov*, 2008]. Aerosols play a  
22 critical role in the interpretation of lunar eclipses as their content, distribution and opti-  
23 cal properties are largely unpredictable. Volcanic eruptions and meteor showers are two  
24 natural sources of aerosols with the potential for perturbing the atmosphere and, in turn,  
25 the aspect of the eclipsed Moon [*Keen*, 1983; *Vollmer and Gedzelman*, 2008]. Occasionally,  
26 large wildfires may also perturb the atmosphere [*Fromm et al.*, 2010].

27 *García Muñoz and Pallé* [2011] have revisited the lunar eclipse theory and estimated the  
28 impact of volcanic aerosols on the spectrum of sunlight at the eclipsed Moon. Aerosols may  
29 substantially attenuate the direct sunlight while simultaneously enhancing somewhat the  
30 scattered contribution. The latter depends strongly on the capacity of aerosols for forward-  
31 scattering the incident light and, consequently, on the aerosols' size. The spectroscopic  
32 characterization of the sunlight reflected from the eclipsed Moon takes the investigation  
33 of lunar eclipses farther than allowed for by photometry and the traditional color indices.

34 The 7–8 August 2008 eruption of the Kasatochi volcano (52.17°N, 175.51°W, Aleutian  
35 Islands, Alaska) ended a period of global low stratospheric aerosol amounts. The three  
36 main explosions recorded over two days plus the release of gas that followed for hours  
37 delivered into the atmosphere  $\sim 1.5$  Tg of SO<sub>2</sub> [*Waythomas et al.*, 2010], which is  $\sim 30$   
38 times less than the SO<sub>2</sub> injected by Pinatubo in 1991. The plume of gas and ash rose up

39 to  $\sim 14$ – $18$  km and drifted eastward carried by jet winds, spreading rapidly over North  
40 America, Greenland, and the North Atlantic Ocean. The cloud was spotted above Europe  
41 on 15 August, one week after the eruption [*Martinsson et al.*, 2009].

42 Our paper shows that a published spectrum of the Moon in umbra during the August  
43 2008 lunar eclipse contains sunlight scattered at the Earth’s terminator. We argue that the  
44 Kasatochi eruption is the most plausible origin for the abnormally elevated atmospheric  
45 opacity needed to explain the observation. *Vidal-Madjar et al.* [2010] have published a  
46 spectrum of the August 2008 lunar eclipse, but covering only the penumbra.

## 2. Data

47 We use data of the 16 August 2008 lunar eclipse obtained with the ALFOSC instrument  
48 mounted on the Nordic Optical Telescope at the Observatorio del Roque de los Muchachos  
49 (La Palma, Spain) and presented by *Pallé et al.* [2009]. The dataset comprises spectra  
50 of the Moon in umbra (21:36UT), penumbra (22:11UT), and out of eclipse (23:09UT).  
51 *Pallé et al.* [2009] derived a lunar eclipse spectrum from the ratio of umbra and penumbra  
52 spectra. The ratio cancels out the solar spectrum and the telluric signature of the Moon-  
53 to-telescope optical path. What remains is the imprint of the limb-viewed terrestrial  
54 atmosphere (averaged in a particular way over the terminator) on the sunlight that reaches  
55 the Moon in umbra. Our analysis sets out from the 400–900 nm published spectrum.

56 The solar elevation angle,  $e$ , is the geocentric angle between the incident sunbeam  
57 direction and the direction from the Earth’s centre to the lunar disk parcel targeted by  
58 the telescope. We have that  $e \sim 0.34^\circ$  for the slit projected on the Moon. The structure of  
59 an umbra spectrum is very sensitive to  $e$  [*García Muñoz and Pallé*, 2011].

### 3. Evidence of scattered sunlight

#### 3.1. The short-wavelength tail of the spectrum

60 Model predictions for  $e \sim 0.34^\circ$  and a broad range of aerosol loadings show that the  
 61 spectrum of sunlight directly transmitted through the atmosphere is typically 2–3 orders  
 62 of magnitude fainter at 400 nm than at 600 nm [*García Muñoz and Pallé, 2011*]. This  
 63 is at odds with the eclipse data, which show that the measured spectrum is roughly flat  
 64 to within a factor of 2 shortwards of 600 nm and that the fluxes at 400 and 880 nm are  
 65 in a ratio of  $\sim 1:20$ . It thus means that direct sunlight is not the only contributor to the  
 66 measured spectrum. *García Muñoz and Pallé [2011]* note that a flat spectrum at short  
 67 wavelengths indicates that diffuse sunlight dominates locally over direct sunlight.

#### 3.2. The $(\text{O}_2)_2$ bands at 577 and 630 nm

68 We fitted synthetic curves of the form  $\prod_i \exp(-\tau_i)$  to the measured spectrum from  
 69 550 to 660 nm. The curves include absorption by  $\text{H}_2\text{O}$ ,  $\text{O}_3$ ,  $\text{O}_2$  and the  $(\text{O}_2)_2$  collisional  
 70 complex. One term,  $\tau_{\text{cont}} = \sum_{k=0}^4 c_k (\lambda_*/\lambda)^k$ , with  $\lambda_* = 600$  nm, accounts for a continuum  
 71 baseline. Thus, each curve contains up to ten degrees of freedom, namely, five  $c_k$ 's,  
 72 integrated columns for  $\text{H}_2\text{O}$ ,  $\text{O}_3$  and  $\text{O}_2$ , and, optionally, one integrated column for each  
 73 of the  $[X^3\Sigma_g^-(0)]_2 \rightarrow a^1\Delta_g(0) + a^1\Delta_g(1)$  and  $[X^3\Sigma_g^-(0)]_2 \rightarrow [a^1\Delta_g(0)]_2$  bands of  $(\text{O}_2)_2$  that  
 74 occur at 577 and 630 nm, respectively. For the temperature-dependent gas properties,  
 75 the temperature was fixed at 225 K. The synthetic curves were properly degraded and  
 76 resampled. The minimization of  $\chi^2 = \sum_j (1 - I_{\text{fit}}(\lambda_j)/I_{\text{exp}}(\lambda_j))^2$ , where  $I_{\text{fit}}$  and  $I_{\text{exp}}$  are the  
 77 synthetic and observed data, outputs the best fit parameters.

78 Figure (1) summarizes the best fits obtained from three separate strategies, each of them  
79 treating the 577 and 630 nm bands of  $(\text{O}_2)_2$  in a different manner. Strategy A fits the  
80 spectrum with null amounts of  $(\text{O}_2)_2$ ; B includes  $(\text{O}_2)_2$  and assumes the same integrated  
81 column for the two bands; and C allows for separate integrated columns for each of the  
82 577 and 630 nm bands. In the top panel, the solid black curves represent the measured  
83 spectrum, shifted in the vertical for comparison with the synthetic curves. The red solid  
84 curves are the respective A, B and C best fits. The bottom panel displays the residuals.  
85 Including  $(\text{O}_2)_2$  reduces notably the fit residuals. The fit improves further if the integrated  
86 column at 630 nm is about twice the column at 577 nm. The latter conclusion is the core  
87 of the second argument that proves the significance of diffuse sunlight in the measured  
88 lunar eclipse spectrum. Some comments on the robustness of the fitting procedure can be  
89 found in the Supplementary Material.

90 Taking C as the optimal strategy, the conclusion is that average sunlight photons at 577  
91 and 630 nm follow different paths in the atmosphere. The direct trajectories of sunlight  
92 rays are dictated by the atmospheric refractive index, which does not change appreciably  
93 within such a narrow spectral interval. The amount of sunlight directly transmitted does  
94 however vary sharply with wavelength. Direct sunlight is more attenuated at 577 nm  
95 than at 630 nm due to the  $\sim\lambda^{-4}$  behaviour of the Rayleigh cross section and the closer  
96 proximity of the 577 nm band to the absorption peak of the  $\text{O}_3$  Chappuis band.

97 We thus have to invoke sunlight scattered at the Earth's terminator to explain the  
98 measured spectrum. *García Muñoz and Pallé* [2011] show that in a lunar eclipse the  
99 bulk of diffuse sunlight near 600 nm originates from above 15 km. In the stratosphere,

100 the  $(\text{O}_2)_2$  density, which drops with a scale height half that of the background density,  
101 is negligibly small. Foreseeably, the signature of the  $(\text{O}_2)_2$  bands in the diffuse sunlight  
102 spectrum is weak.

#### 4. Analysis and discussion

103 Next, we generate model lunar eclipse spectra that reproduce the measured spectrum  
104 if a few reasonable assumptions on the loading and properties of airborne aerosols are  
105 introduced. The spectra, generated with the model described by *García Muñoz and Pallé*  
106 [2011], contain both direct and diffuse components. Further details on the underlying  
107 model assumptions can be found in the Supplementary Material.

108 The tracing of the direct sunbeam that reached the parcel of the Moon's disk tracked  
109 by the telescope reveals that the sunbeam intercepted the volcanic cloud formed in the  
110 Kasatochi eruption, as seen in Fig. (2). It is expected that the direct sunlight component  
111 is more strongly affected by the volcanic cloud than the diffuse one, which originates from  
112 all terminator locations. This distinction is accounted for in the generation of the model  
113 spectra by assuming separate atmospheres for the calculation of each component.

114 For simplicity, the model spectra are allowed only four adjustable parameters. These  
115 are  $f_{\gamma_0}$ ,  $\alpha'$  and  $f_{\text{O}_3}$  for the direct sunlight component, and  $r_{\text{eff}}$  for the diffuse one. In the  
116 former,  $f_{\gamma_0}$  scales the reference aerosol extinction profile at  $1.02 \mu\text{m}$ ,  $\alpha'$  is the Ångström  
117 exponent to extrapolate the  $1.02\text{-}\mu\text{m}$  extinction profile to shorter wavelengths, and  $f_{\text{O}_3}$   
118 scales the reference ozone profile. In the calculation of the diffuse sunlight component,  $r_{\text{eff}}$   
119 stands for a mean effective radius for aerosols at the terminator. The sulfate droplets of  
120 background aerosols in the quiescent atmosphere have  $r_{\text{eff}} \sim 0.1\text{--}0.2 \mu\text{m}$ , whereas volcanic

121 ash particles with residence times longer than a few days may have  $r_{\text{eff}}$ 's of a few microns  
122 [*Bauman et al.*, 2003; *Muñoz et al.*, 2004]. *Sioris et al.* [2010] report  $r_{\text{eff}}$ 's of  $\sim 0.6 \mu\text{m}$   
123 for September 2008, which are indicative of a perturbed atmosphere. It is unclear what  
124 the mean  $r_{\text{eff}}$  at the terminator was one week after the eruption. Thus, we explored a set  
125 of  $r_{\text{eff}}$  from 0.1 to 2  $\mu\text{m}$  to bracket possible sizes. A large  $r_{\text{eff}}$  results in phase functions  
126 strongly peaked in the forward direction.

127 For each  $r_{\text{eff}}$ , one diffuse sunlight spectrum was produced. For each diffuse spectrum an  
128 algorithm seeks the  $f_{\gamma_0}$ ,  $\alpha'$  and  $f_{\text{O}_3}$  values producing the best fit of the direct + diffuse  
129 model spectra to the continuum of the measured spectrum. The algorithm forces the  
130 (flux-uncalibrated) measured spectrum to match the model spectra at 875 nm. Figure (3)  
131 shows the best fit for  $r_{\text{eff}}=0.5 \mu\text{m}$  and the values inferred for the other three adjustable  
132 parameters. The  $a$  parameter is the multiplicative factor to pass from the normalization in  
133 the graph to the Earth-to-Sun ratio as discussed by *García Muñoz and Pallé* [2011]. Figure  
134 (I) in the Supplementary Material shows the best fits for the full  $r_{\text{eff}}$  set. It is apparent  
135 the good *a posteriori* match of the  $\text{O}_2$  bands in all cases. The differences between the  
136 measured spectrum and the best fits are of a few percent longwards of 600 nm, but of  
137  $\sim 50\%$  near 500 nm. This is a consequence of fitting the measured spectrum with models  
138 that contain a reduced number of adjustable parameters. The residuals longwards of 700  
139 nm are mainly due to a known instrumental issue of uncorrected fringing.

140 The  $f_{\gamma_0}$  values inferred point to heavy aerosol loadings with peak extinctions of  $\sim 10^{-2}$   
141  $\text{km}^{-1}$  in the atmosphere intercepted by the direct sunbeam. Comparable extinctions  
142 were reported on global scales for a few months after the Pinatubo eruption [*Bauman*



143 *et al.*, 2003]. Exponents  $\alpha' \sim 0-0.15$  are indicative of large-size particles being carried in  
144 the volcanic cloud. The conversion from  $\text{SO}_2$  to sulfate droplets has an e-folding time  
145 of 20–50 days [*Kristiansen et al.*, 2010]. It is unlikely that one week after the eruption  
146 is enough time for large sulfate droplets to form. Thus, the  $\alpha'$  values inferred suggest  
147 that the volcanic cloud carried sizeable amounts of un-sedimented ash. *Sioris et al.* [2010]  
148 report small Ångström exponents of  $\sim 0.5$  in early September 2008.

149 The inset of Fig. (3) shows the two component spectra near 600 nm. The diffuse  
150 spectrum is roughly flat and shows no evidence of  $(\text{O}_2)_2$  absorption. When the direct and  
151 diffuse model spectra are added, the 577 nm band becomes more diluted than the 630  
152 nm band, which translates into an effective integrated column at 630 nm larger than at  
153 577 nm. For the case in Fig. (3) the ratio is  $\sim 1:1.4$ , somewhat smaller than the  $\sim 1:2$   
154 ratio inferred from the measured spectrum. One may generally state that comparable  
155 amounts of direct and scattered sunlight near 600 nm lead to larger  $(\text{O}_2)_2$  columns at the  
156 longer-wavelength band.

157 Figure (I) in the Supplementary Material proves that good fits to the measured spectrum  
158 are possible for the full  $r_{\text{eff}}$  set. This means that the measured spectrum accepts one  
159 quantitative interpretation for each  $r_{\text{eff}}$ . In qualitative terms, though, the picture that  
160 we obtain is fairly consistent and indicates that the direct sunbeam was substantially  
161 attenuated by the volcanic cloud, which leads to an enhanced contrast of the diffuse  
162 component. For future efforts, we suggest that the flux calibration of the undivided  
163 spectra might help break the degeneracy.

164 A comment is to be made regarding the Ring effect and the structure seen in the mea-  
165 sured spectrum shortwards of 540 nm. The Ring effect refers to the smearing of solar  
166 Fraunhofer lines that occurs in the spectrum of sunlight scattered in the atmosphere  
167 [*Grainger and Ring*, 1962]. In the Earth’s atmosphere, the Ring effect is due to rotational  
168 Raman scattering by N<sub>2</sub> and O<sub>2</sub> [*Kattawar et al.*, 1981]. Raman scattering redistributes in  
169 wavelength part of the incident photons, the redistribution being more evident where the  
170 incident solar spectrum shows the sharpest lines. The ratio of scattered to unscattered  
171 sunlight spectra reveals the Ring effect as a filling-in of the solar line cores. The detection  
172 of the Ring effect in the eclipse data would mean a further confirmation of scattered sun-  
173 light. The measured lunar eclipse spectrum shows that ripples do occur in the Fraunhofer  
174 region. The sign of the structures is however inverted with respect to what the Ring effect  
175 would produce. The inspection of the undivided umbra spectrum shows that the solar  
176 lines are unexpectedly deep, probably due to the limitation in the subtraction of the sky  
177 spectrum at these wavelengths, where the signal-to-noise ratio is the lowest. Thus, the  
178 structure seen in the measured spectrum cannot be attributed to the Ring effect. Further,  
179 a few quantitative arguments allow us to deem as minor the impact of the Ring effect on  
180 the measured lunar eclipse spectrum. Following *Kattawar et al.* [1981], the filling-in for  
181 forward-scattered sunlight is  $\sim 2.5\%$  of the continuum Rayleigh-scattered by the gas. In  
182 the conditions explored here the filling-in would be undetectably small because the sun-  
183 light scattered by the gas contributes less than a few percent to the net sunlight scattered  
184 by gas and aerosols together.

185 Pyrocumulonimbus (pyroCbs) is a recently-coined term to designate convective activity  
186 triggered or sustained by wildfires [*Fromm et al.*, 2010]. In extreme events, pyroCbs inject  
187 smoke and biomass-burning particles into the troposphere and lower stratosphere and alter  
188 the global aerosol loading. PyroCbs may result in aerosol extinctions  $\sim 10^{-3}$ – $10^{-2}$  km<sup>-1</sup>  
189 well above the tropopause, opacities that are often associated with volcanic clouds. It  
190 would be difficult to differentiate the impact on the eclipsed Moon of one such event from  
191 that of a volcanic eruption. To our knowledge, no extreme pyroCbs were reported in  
192 the weeks preceding the eclipse, a period that was monitored with unprecedented detail.  
193 Thus, if any, the contribution in the eclipse of pyroCbs blended with that of the Kasatochi  
194 cloud.

195 The Perseids is one of the most copious meteor showers, running yearly from late July  
196 to late August. In 2008, its peak of activity occurred near 13 August. Despite recent  
197 work [*Matshvili et al.*, 1999; *Renard et al.*, 2010], there are significant uncertainties on  
198 the optical properties of the atmosphere perturbed by meteor showers. *Matshvili et al.*  
199 [1999] report two-fold enhancements with respect to pre-shower values in the twilight  
200 brightness above 20 km during the Leonids in 1998. Assuming that both meteor showers  
201 are comparable and that the brightness enhancement translates into a similar increase in  
202 stratospheric opacity, the effect of extraterrestrial dust would be more than one order of  
203 magnitude smaller than that by the volcanic perturbation. Thus, the effect of meteoroid  
204 dust in the measured spectrum is likely masked by the volcanic perturbation.

205 We have shown that the lunar eclipse spectrum published by *Pallé et al.* [2009] was  
206 affected by sunlight scattered at the Earth’s terminator. We offered theoretical arguments

207 that hint at the Kasatochi eruption as the most plausible origin for the atmospheric  
208 perturbation needed to explain the observations. Future observations will allow us to  
209 compare lunar eclipse spectra obtained in different atmospheric conditions. In a broader  
210 context, it is worth mentioning that the retrieval of globally-averaged atmospheric optical  
211 properties is a relevant exercise towards the future characterization of transiting Earth-  
212 like extrasolar planets. As a corollary, we may state that the color of the lunar disk in  
213 umbra during the 16 August 2008 lunar eclipse was partly caused by diffuse sunlight.

214 **Acknowledgments.** ELM acknowledges a Visiting Research Professorship at the De-  
215 partment of Geological Sciences of the University of Florida. We thank the two reviewers  
216 for constructive comments.

## References

- 217 Bauman, J.J., P. B. Russell, M. A. Geller, and P. Hamill (2003), A stratospheric aerosol  
218 climatology from SAGE II and CLAES measurements: 2. Results and comparisons,  
219 1984–1999, *J. Geophys. Res.*, *108*, 4383, doi:10.1029/2002JD002993.
- 220 Fromm, M., D.T. Lindsey, R. Servranckx, G. Yue, T. Trickl, R. Sica, P. Doucet, S. Godin-  
221 Beekmann (2010), The untold story of pyrocumulonimbus, *BAMS*, *91*, 1193–1209.
- 222 García Muñoz, A., and E. Pallé (2011), Lunar eclipse theory revisited: Scattered sunlight  
223 in both the quiescent and the volcanically perturbed atmosphere, *JQSRT*, *112*, 1609–  
224 1621.
- 225 Grainger, J.F., and J. Ring (1962), Anomalous Fraunhofer line profiles, *Nature*, *193*, 762.

- 226 Kattawar, G.W., A.T. Young, and T.J. Humphreys (1981), Inelastic scattering in plane-  
227 tary atmospheres. I. The Ring effect, without aerosols, *Astrophys. J.*, *243*, 1049–1057.
- 228 Keen, R. (1983), Volcanic aerosols and lunar eclipses, *Science*, *222*, 1011–1013.
- 229 Kristiansen, N.I., A. Stohl, A.J. Prata, A. Richter, S. Eckhardt, et al. (2010), Remote  
230 sensing and inverse transport modeling of the Kasatochi eruption sulfur dioxide cloud,  
231 *J. Geophys. Res.*, *115*, D00L16, doi:10.1029/2009JD013286.
- 232 Link, F. (1962), Lunar eclipses. In: Kopal Z, editor. Physics and Astronomy of the Moon,  
233 p. 161–229.
- 234 Martinsson, B.G., C. A. M. Brenninkmeijer, S. A. Carn, M. Hermann, K.-P. Heue, P.F.J.  
235 van Velthoven, and A. Zahn (2009), Influence of the 2008 Kasatochi volcanic eruption  
236 on sulfurous and carbonaceous aerosol constituents in the lower stratosphere, *Geophys.*  
237 *Res. Lett.*, *36*, L12813, doi:10.1029/2009GL038735.
- 238 Mateshvili, N., G. Mateshvili, I. Mateshvili, L. Gheondjian, and O. Avsajanishvili (1999),  
239 Vertical distribution of dust particles in the Earth’s atmosphere during the 1998 Leonids,  
240 *Meteoritics & Planet. Science*, *34*, 969–973.
- 241 Muñoz, O., H. Volten, J.W. Hovenier, B. Veihelmann, W.J. van der Zande, et al. (2004),  
242 Scattering matrices of volcanic ash particles of Mount St. Helens, Redoubt, and Mount  
243 Spurr volcanoes, *J. Geophys. Res.*, *109*, D16201, doi:10.1029/2004JD004684.
- 244 Pallé, E., M.R. Zapatero Osorio, R. Barrena, P. Montañés-Rodríguez, and E.L. Martín  
245 (2009), Earth’s transmission spectrum from lunar eclipse observations, *Nature*, *459*,  
246 814–816.

- 247 Renard, J.-B., G. Berthet, V. Salazar, V. Catoire, M. Tagger, et al. (2010), In situ de-  
248 tecton of aerosol layers in the middle stratosphere, *Geophys. Res. Lett.*, *37*, L20803,  
249 doi:10.1029/2010GL044307.
- 250 Sioris, C. E., C. D. Boone, P. F. Bernath, J. Zou, C. T. McElroy, and C. A. McLinden  
251 (2010), Atmospheric Chemistry Experiment (ACE) observations of aerosol in the upper  
252 troposphere and lower stratosphere from the Kasatochi volcanic eruption, *J. Geophys.*  
253 *Res.*, *115*, D00L14, doi:10.1029/2009JD013469.
- 254 Ugolnikov, O.S., and I.A. Maslov (2008), Altitude and latitude distribution of atmospheric  
255 aerosol and water vapor from the narrow-band lunar eclipse photometry, *JQSRT*, *109*,  
256 378–388.
- 257 Vidal-Madjar, A., L. Arnold, D. Ehrenreich, R. Ferlet, A. Lecavelier des Etangs, et al.  
258 (2010), The Earth as an extrasolar transiting planet. Earth’s atmospheric composition  
259 and thickness revealed by lunar eclipse observations, *A&A*, *523*, A57.
- 260 Vollmer, M. and S.D. Gedzelman (2008), Simulating irradiance during lunar eclipses: The  
261 spherically symmetric case *Appl. Opt.*, *47*, H52–H61.
- 262 Waythomas, C. F., W. E. Scott, S. G. Prejean, D. J. Schneider, P. Izbekov, and C. J. Nye  
263 (2010), The 7–8 August 2008 eruption of Kasatochi volcano, central Aleutian Islands,  
264 Alaska, *J. Geophys. Res.*, *115*, B00B06, doi:10.1029/2010JB007437.

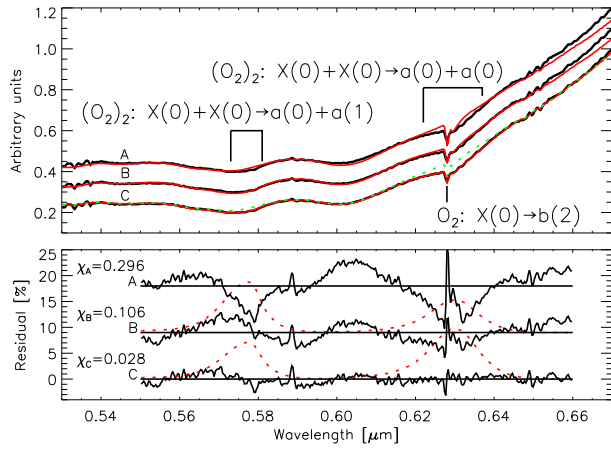


**Figure 1.** Top: Best fits (red) to the measured spectrum (black) from 550 to 660 nm. The dotted green line are the best fits divided by  $\exp(-\tau_{(\text{O}_2)_2})$ . The comparison of the dotted and solid curves makes explicit the contributions from the coincidental in position, albeit distinct in nature,  $\text{O}_2$   $X(0) \rightarrow b(2)$  and  $(\text{O}_2)_2$   $X(0)+X(0) \rightarrow a(0)+a(0)$  absorption bands near 630 nm. Bottom: Fit residuals. For B and C, the dotted red curves are the  $(\text{O}_2)_2$  contributions. In C, we infer an optimal ratio for the 577:630 nm integrated columns of  $\sim 1:2$ .

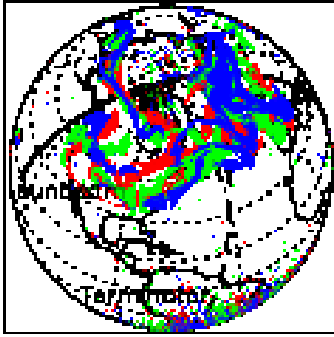


**Figure 2.** Solid: Projected mid-section trajectory of the sunbeam that reaches the lunar disk targeted by the telescope at 21:36UT on 16 August 2008. Overplotted, the SO<sub>2</sub> cloud (a usual volcanic cloud tracer) on 15, 16 and 17 August (red, green and blue, respectively) according to AURA/OMI data (downloaded from the Giovanni online data system, developed and maintained by the NASA GES DISC). The sunbeam’s closest approach to the Earth’s surface occurs in the North Atlantic region. The local tropopause is at  $\sim 10$  km. Dashed: Line of the terminator.

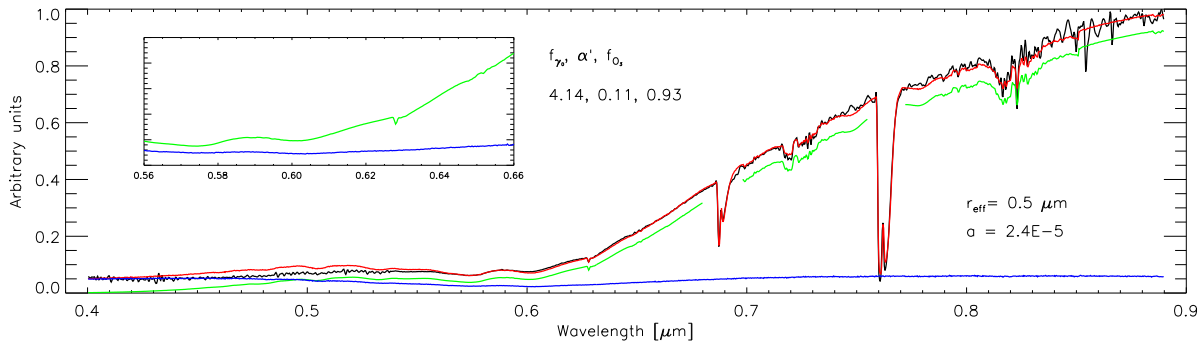


**Figure 3.** Best model fit for  $r_{\text{eff}}=0.5 \mu\text{m}$  (red) to the measured spectrum (black). The model spectrum contains contributions from direct sunlight (green) and diffuse sunlight (blue). The inset is a zoom of the region near 600 nm. The algorithm aims the fit of the continuum away from O<sub>2</sub> and H<sub>2</sub>O bands. The H<sub>2</sub>O bands were fitted separately after the fit to the continuum. Figure (I) in the Supplementary Material shows the best fits for the full set of  $r_{\text{eff}}$  values.



## Supplementary material

### Additional comments on the robustness of the fitting procedure of Section 3

Our fitting algorithm uses the laboratory measurements for  $(\text{O}_2)_2$  cross sections by Greenblatt et al. (1990). Later experiments [Newnham and Ballard, 1998; Naus and Ubachs, 1999] and transmitted moonlight measurements [Wagner et al., 2002] have confirmed that the Greenblatt et al. (1990) cross sections are correct to within a few percent. We verified that using the Newnham and Ballard (1998) cross sections does not modify our conclusion that strategy C performs better than strategies A and B. The conclusion remains also unchanged if an alternative temperature in the range 200–250 K is used to evaluate the temperature-dependent optical properties of the absorbing gases.

### Additional information on the spectra simulations of Section 4

A thorough description of the model used in Section 4 can be found in García Muñoz and Pallé (2011). Vertically-resolved optical properties of the atmosphere are input to the model. The model also requires the scattering phase functions of all airborne particles. Then, for a selected solar elevation angle, it produces both direct and diffuse spectra of the sunlight arriving at the Moon normalized to the net solar irradiance.

We follow García Muñoz and Pallé (2011) for the temperature and densities of the spectroscopically active molecules in the spectral region of investigation (mainly  $\text{H}_2\text{O}$ ,  $\text{O}_2$  and  $\text{O}_3$ ). The composite global map of cloud top heights retrieved from GOME-2 data (ICSU World Data Center for Remote Sensing of the Atmosphere, <http://wdc.dlr.de/>) shows for 16 August 2008 clouds with top heights between 4 and 10 km at 50–70°N latitudes. In the direct sunlight calculation, we assume that clouds block the sunlight below 6 km. A precise choice of the cloud top height is not critical because for elevated aerosol loadings the atmosphere at that altitude is optically thick in limb viewing. Most of the diffuse sunlight is scattered from higher altitudes, and the choice of the cloud top height in the calculation of the diffuse component is less important.

Several works have investigated the optical properties of the post-eruption atmosphere [e.g., Bourassa et al., 2010; Hoffmann et al., 2010]. Sioris et al. (2010) have produced 1.02- $\mu\text{m}$  extinction profiles from solar occultation data obtained with the Atmospheric Chemistry Experiment (ACE) Imager. The September 2008 ACE Imager extinction profile peaks at altitudes of  $\sim 9$  and 15 km, and has an integrated optical thickness above 6 km of  $\sim 0.02$ , notably larger than the optical thickness for the same month from 2004 to 2007. It must be noted that the September 2008 ACE Imager extinction profile (hereafter referred to as  $\gamma_0(\lambda_0, z)$ ) was inferred from data gathered 2–7 weeks after the eclipse and includes measurements taken over the entire northern hemisphere. Thus,  $\gamma_0(\lambda_0, z)$  is not directly applicable to the interpretation of the measured lunar eclipse spectrum.

For our direct sunlight calculations, we take as extinction profile by aerosols  $\gamma(\lambda, z) = f_{\gamma_0} \gamma_0(\lambda_0, z) (\lambda/\lambda_0)^{\alpha}$ , where  $f_{\gamma_0}$  is a mere scaling factor and  $\alpha$  is a so-called Ångström exponent. Typically,  $\alpha$  ranges from 0, for particles much larger than the incident photon wavelength, to 4, in the limit of molecule-sized particles. We also allow for ozone extinction in the 400–850 nm region of the Chappuis band. For this, we take the reference ozone profile of García Muñoz and Pallé (2011) and scale it by an additional parameter  $f_{\text{O}_3}$ . A battery of  $17 \times 5 \times 5 = 425$  direct sunlight spectra was created to sample the  $f_{\gamma_0} - \alpha - f_{\text{O}_3}$  parameter space in the  $[0, 8] - [0, 2] - [0, 2]$  intervals. These spectra are mainly intended to reproduce the continuum of the measured spectrum away from molecular bands.

As a check, it is worth noting that the values retrieved for  $f_{\text{O}_3}$  in the fits of the Section 4 range from 0.85 to 0.95, which mean (for a reference profile of  $\sim 360$  Dobson Units of vertically-integrated ozone) ozone columns between 306 and 342 DU. The total ozone map for 16 August 2008 (World Ozone and Ultraviolet Radiation Data Centre, WOUDC, <http://www.woudc.org>) shows that in the North Atlantic region near Greenland, where the sunbeam intercepts the terminator, the ozone

column is 300–350 DU. Thus, the ozone columns reported at WOUDC and our own retrieved columns are in reasonable agreement.

Our diffuse sunlight calculations use the September 2007 ACE Imager extinction profile as representative of background aerosols. The profile is somewhat arbitrarily multiplied by 1.5 to account for some post-eruption global aerosol enhancement. Shortwards of  $1.02\ \mu\text{m}$ , we infer the extinctions by means of an Ångström-type law with an exponent of 1 appropriate to a weakly-to-moderately perturbed atmosphere [Hayashida and Horikawa, 2001]. The total ozone map for 16 August 2008 shows that at the Earth's terminator the average ozone column was less than in our reference profile. Thus, for the diffuse sunlight calculations we have re-scaled the reference profile to a total ozone column of  $\sim 250$  Dobson Units.

The phase function of airborne particles at the small scattering angles that occur for forward-, single-scattered sunlight photons is critical in the diffuse problem. Multiple processes, which include sedimentation, advection, condensation and coagulation, govern the aerosols' evolving size distribution in the weeks and months after an eruption. It is not known a priori the average global value of  $r_{\text{eff}}$  on the date of the eclipse. Thus, we decided to explore the set of  $r_{\text{eff}}$  values: 0.1, 0.2, 0.5, 1.0 and  $2.0\ \mu\text{m}$ . A size of  $r_{\text{eff}} \sim 0.1\ \mu\text{m}$  is representative of an unperturbed atmosphere, whereas  $r_{\text{eff}} \sim 2\ \mu\text{m}$  would mean that the entire terminator is rich in fresh ash. In going from  $r_{\text{eff}} = 0.1$  to  $2\ \mu\text{m}$ , the phase function in the forward direction (calculated from Mie theory for a unimodal log-normal size distribution, a geometric standard deviation of 2 and a refractive index of 1.45, M. Mishchenko, [www.giss.nasa.gov/staff/mmishchenko/t\\_matrix.html](http://www.giss.nasa.gov/staff/mmishchenko/t_matrix.html)) augments by  $\sim 20$ . The phase functions are calculated at a few wavelengths and interpolated in between.

### **Bibliography for the Supplementary Material**

Bourassa, A. E., D. A. Degenstein, B. J. Elash, and E. J. Llewellyn (2010), Evolution of the stratospheric aerosol enhancement following the eruptions of Okmok and Kasatochi: Odin – OSIRIS measurements, *J. Geophys. Res.*, 115, D00L03, doi:10.1029/2009JD013274.

García Muñoz, A., and E. Pallé (2011), Lunar eclipse theory revisited: Scattered sunlight in both the quiescent and the volcanically perturbed atmosphere, *JQSRT*, in press.

Greenblatt, G.D., J.J. Orlando, J.B. Burkholder, and A.R. Ravishankara (1990), Absorption measurements of oxygen between 330 and 1140 nm, *J. Geophys. Res.*, 95, 18577 – 18582.

Hayashida, S., and M. Horikawa (2001), Anti-correlation between stratospheric aerosol extinction and the Ångström parameter from multiple wavelength measurements with SAGE II – a characteristic of the decay period following major volcanic eruptions, *Geophys. Res. Lett.*, 28, 4063–4066.

Hoffmann, A., C. Ritter, M. Stock, M. Maturilli, S. Eckhardt, et al. (2010), Lidar measurements of the Kasatochi aerosol plume in August and September 2008 in Ny-Ålesund, Spitsbergen, *J. Geophys. Res.*, 115, doi:10.1029/2009JD013039.

Naus, H., and W. Ubachs (1999), Visible absorption bands of the  $(\text{O}_2)_2$  collision complex at pressures below 760 Torr, *Appl. Optics*, 38, 3,423 – 3,428.

Newnham, D.A., and J. Ballard (1998), Visible absorption cross sections and integrated absorption intensities of molecular oxygen ( $\text{O}_2$  and  $\text{O}_4$ ), *J. Geophys. Res.*, 103, 28,801 – 28,816.

Sioris, C. E., C. D. Boone, P. F. Bernath, J. Zou, C. T. McElroy, and C. A. McLinden (2010), Atmospheric Chemistry Experiment (ACE) observations of aerosol in the upper troposphere and lower stratosphere from the Kasatochi volcanic eruption, *J. Geophys. Res.*, 115, D00L14, doi:10.1029/2009JD013469.

Wagner, T., C. von Friedeburg, M. Wenig, C. Otten, and U. Platt (2002), UV-visible observations of atmospheric  $\text{O}_4$  absorptions using direct moonlight and zenith-sky sunlight for clear-sky and cloudy sky conditions, *J. Geophys. Res.*, 107, 4424, doi:10.1029/2001JD001026.

Figure mentioned in the main text.

